Hindawi Publishing Corporation
ISRN Thermodynamics
Volume 2013, Article ID 108264, 9 pages
http://dx.doi.org/10.1155/2013/108264

Research Article

Analytical Solution of MHD Stagnation-Point Flow and Heat Transfer of Casson Fluid over a Stretching Sheet with Partial Slip

Samir Kumar Nandy

Department of Mathematics, A.K.P.C Mahavidyalaya, Bengai, Hooghly 712 611, India

Correspondence should be addressed to Samir Kumar Nandy; nandysamir@yahoo.com

Received 21 June 2013; Accepted 13 July 2013

Academic Editors: R. R. Burnette and I. Kim

This paper investigates the hydromagnetic boundary layer flow and heat transfer of a non-Newtonian Casson fluid in the neighborhood of a stagnation point over a stretching surface in the presence of velocity and thermal slips at the boundary. The governing partial differential equations are transformed into nonlinear ordinary differential equations using similarity transformations. The analytic solutions are developed by a homotopy analysis method (HAM). The results pertaining to the present study indicate that the flow and temperature fields are significantly influenced by Casson parameter (β), the magnetic parameter M, the velocity slip parameter δ, and the thermal slip parameter γ. An increase in the velocity slip parameter δ causes decrease in the flow velocity, while an increase in the value of the thermal slip parameter γ causes increase in the temperature of the fluid. It is also observed that the velocity at a point decreases with increase in β.

1. Introduction

The problems of flow and heat transfer in the boundary layer adjacent to a continuous moving surface have received great attention during the last decades owing to the abundance of practical applications in chemical and manufacturing processes, such as polymer extrusion, continuous casting of metals, glass fibre production, hot rolling of paper, and wire drawing. Sakiadis [1] was the first, among others, to investigate the flow behavior on continuous solid surface. Thereafter, numerous investigations were made on the flow and heat transfer over a stretching surface in different directions [2–8].

All the previous researchers restricted their analyses to flow and heat transfer for the Newtonian fluid. In recent years, it has been observed that a number of industrial fluids such as molten plastics, polymeric liquids, blood, food stuff, and slurries exhibit non-Newtonian fluid behavior. Different types of non-Newtonian fluids are viscoelastic fluid, couple stress fluid, micropolar fluid, power-law fluid, Casson fluid, and many others. Rajagopal et al. [9] and Siddappa and Abel [10] studied the flow of a viscoelastic fluid over a linear stretching sheet. Troy et al. [11], Lawrence and Rao [12], and McLeod and Rajagopal [13] discussed the problem of uniqueness/nonuniqueness of the flow of a non-Newtonian viscoelastic fluid over a stretching sheet. Rajagopal et al. [9] analyzed the solutions for the flow of viscoelastic fluid over a stretching sheet. This study was further generalized to investigate the flow of short memory fluid of type Walter's liquid B by several authors, such as Andersson [14], Rollins and Vajravelu [15], and Abel and Veena [16].

Although different models are proposed to explain the behavior of non-Newtonian fluids, the most important non-Newtonian fluid possessing a yield value is the Casson fluid. This fluid has significant applications in polymer processing industries and biomechanics. We can define a casson fluid as a shear thinning fluid which is assumed to have an infinite viscosity at zero rate of shear. Casson's constitutive equations are found to describe accurately the flow curves of suspensions of pigments in lithographic varnishes used for preparation of printing inks and silicon suspensions [17]. Various experiments performed on blood with varying haematocrits, anticoagulants, temperatures, and so forth strongly suggest the behavior of blood as a casson fluid [18–20]. In particular, casson fluid model describes the flow

characteristics of blood more accurately at low shear rates and when it flows through small vessels [21].

Fluid flow in microelectromechanical systems (MEMS) has become an interesting topic because in microscale dimensions, the fluid flow behavior deviates significantly from the traditional no-slip flow. Under the microscale dimensions, the fluid motion still obeys the Navier-Stokes equations but under slip velocity boundary conditions. For large scale problems with low density, the fluid can be modeled as a rarefied gas, and rarefied gas flows with slip boundary conditions are often countered in the microscale devices. The nonadherence of the fluid to a solid boundary, known as velocity slip, is a phenomenon observed in certain circumstances. Partial slips occur for fluids with particulate such as emulsions, suspensions, foams, and polymer solutions. Fluids exhibiting slip are important in technological applications such as in the polishing of artificial heart valves and internal cavities. With a slip at the wall boundary, the flow behavior and the shear stress in the fluid are quite different from those in the no-slip flows. The slip flows in different flow configurations were studied in recent years (see [22–27]). The MHD flow under slip conditions over a permeable shrinking surface was solved analytically by Fang et al. [28], and they reported that the velocity slip at the shrinking surface greatly affects the velocity distribution and drag forces on the wall. Bhattacharyya et al. [29] studied the effects of partial slip on the boundary layer stagnation-point flow and heat transfer towards a shrinking surface. The slip effect on MHD boundary layer flow over a flat plate was also considered by Bhattacharyya et al. [30]. Ariel et al. [31] considered the flow of a viscoelastic fluid over a stretching sheet with partial slip, and Ariel [32] also studied the slip effect on stagnation-point flow of an elasticoviscous fluid over a wall. Fang et al. [33] obtained the exact analytic solution of MHD flow under slip condition over a permeable stretching sheet.

However, in the literature, articles are not available on the MHD boundary layer stagnation-point flow of a casson fluid over a stretching sheet. The present paper aims to study the slip effect on MHD boundary layer flow and heat transfer of a casson fluid over a stretching sheet using the homotopy analysis method (HAM) which is successively applied to various interesting problems [34–41]. The self-similar equations are solved analytically by HAM for a range of values of the physical parameters. The results obtained are then compared with those from the available literature for some particular values of the physical parameters, and it is found that they are in a good agreement. The results pertaining to the present study indicate that the flow and the temperature fields are greatly influenced by the velocity and thermal slip parameters.

2. Flow Analysis

Consider the steady magnetohydrodynamic (MHD) flow of a non-Newtonian Casson fluid near the stagnation point over a stretching surface coinciding with the plane $y = 0$, the flow being confined to $y > 0$. Two equal and opposite forces are applied along the x-axis so that the surface is stretched

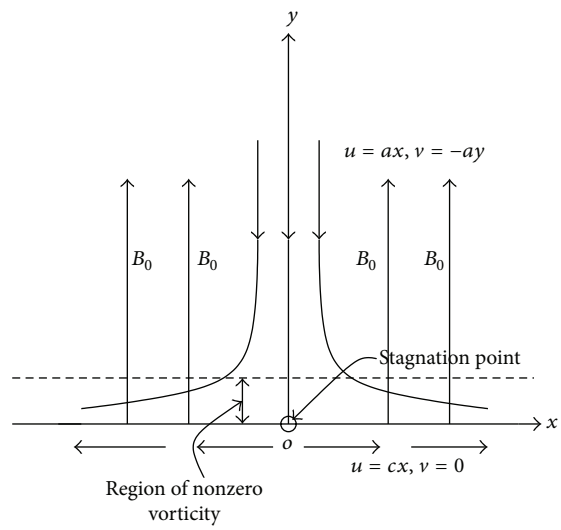

Figure 1: A physical model and the coordinate system.

keeping the origin fixed. A uniform magnetic field of strength B_0 is applied in a direction normal to the surface. It is assumed that the velocity distribution far from the surface is given by $u \to U(x) = ax$, where $a(>0)$ is a constant. The stretching surface has a uniform temperature T_w and the temperature far away from the surface is T_∞. The flow configuration is shown in Figure 1.

The rheological equation of state for an isotropic and incompressible flow of a Casson fluid can be written as, see Nakamura and Sawada [42],

$$\tau_{ij} = 2\left(k_c + \frac{\tau_0}{\sqrt{2\pi}}\right)e_{ij}, \quad \pi > \pi_c,$$
$$\tau_{ij} = 2\left(k_c + \frac{\tau_0}{\sqrt{2\pi_c}}\right)e_{ij}, \quad \pi < \pi_c, \tag{1}$$

where

$$e_{ij} = \frac{1}{2}\left(\frac{\partial u_i}{\partial x_j} + \frac{\partial u_j}{\partial x_i}\right) \tag{2}$$

is the rate-of-strain tensor, k_c is the Casson's coefficient of viscosity, π is the product of the component of deformation rate with itself, π_c is the critical value of the product of the component of the rate-of-strain tensor with itself, τ_0 is the yield stress of the fluid, and u_i are the velocity components.

The MHD equations for this problem in the boundary layer near the stretching surface are

$$\frac{\partial u}{\partial x} + \frac{\partial v}{\partial y} = 0, \tag{3}$$

$$u\frac{\partial u}{\partial x} + v\frac{\partial u}{\partial y} = U\frac{dU}{dx} + \nu\left(1 + \frac{1}{\beta}\right)\frac{\partial^2 u}{\partial y^2} + \frac{\sigma B_0^2}{\rho}(U - u), \tag{4}$$

$$u\frac{\partial T}{\partial x} + v\frac{\partial T}{\partial y} = \kappa\frac{\partial^2 T}{\partial y^2} + \frac{\nu}{c_p}\left(1 + \frac{1}{\beta}\right)\left(\frac{\partial u}{\partial y}\right)^2 + \frac{\sigma B_0^2}{\rho c_p}(U - u)^2, \tag{5}$$

where u and v are the velocity components along the x and y directions, respectively, ρ is the density of the fluid, σ is the electrical conductivity, B_0 is the uniform magnetic field along y-axis, κ is the thermal diffusivity, c_p is the specific heat at constant pressure, ν is the kinematic viscosity, and $\beta(=k_c\sqrt{2\pi_c}/\tau_0)$ is the Casson parameter. In writing (4), we have neglected the induced magnetic field since the magnetic Reynolds number R_M for the flow is assumed to be very small. This assumption is justified for flow of electrically conducting fluids such as liquid metals, for example, mercury, liquid sodium, and so forth (Shercliff [43]).

The slip boundary conditions for the problem are

$$\begin{gathered} u = cx + L\frac{\partial u}{\partial y}, \quad v = 0, \quad T = T_w + S\frac{\partial T}{\partial y} \quad \text{at } y = 0, \\ u \longrightarrow U(x) = ax, \qquad T \longrightarrow T_\infty \quad \text{as } y \longrightarrow \infty, \end{gathered} \tag{6}$$

where L is the velocity slip factor, S is the thermal slip factor, and $a(>0)$, $c(>0)$ are constants. For $L = 0$ and $S = 0$, no-slip condition can be recovered.

The continuity equation can be satisfied by introducing a stream function ψ such that

$$u = \frac{\partial \psi}{\partial y}, \qquad v = -\frac{\partial \psi}{\partial x}. \tag{7}$$

The momentum and energy equations can be transformed into the corresponding nonlinear ordinary differential equations by the following transformations:

$$\psi = x\sqrt{c\nu}F(\eta), \quad \theta(\eta) = \frac{T - T_\infty}{T_w - T_\infty}, \quad \eta = y\sqrt{\frac{c}{\nu}}, \tag{8}$$

where η is the independent similarity variable and where $T_w - T_\infty = bx^2$, b is a positive constant. Using these relations, we get the transformed nonlinear ordinary differential equations from (4) and (5) as

$$\left(1 + \frac{1}{\beta}\right)F''' + FF'' - F'^2 + \alpha^2 + M\left(\alpha - F'\right) = 0, \tag{9}$$

$$\frac{1}{\Pr}\theta'' + F\theta' - 2F'\theta + \left(1 + \frac{1}{\beta}\right)E_cF'' + ME_c\left(\alpha - F'\right)^2 = 0, \tag{10}$$

where $\alpha(=a/c)$ is the dimensionless velocity ratio parameter, $M(=\sigma B_0^2/\rho c)$ is the magnetic parameter, $\Pr = (\nu/\kappa)$ is the Prandtl number, $E_c(=c^2/bc_p)$ is the Eckert number, and a prime denotes differentiation with respect to the similarity variable η. The transformed boundary conditions for $F(\eta)$ and $\theta(\eta)$ are

$$\begin{gathered} F(0) = 0, \quad F'(0) = 1 + \delta F''(0), \quad \theta(0) = 1 + \gamma\theta'(0), \\ F'(\infty) = \alpha, \quad \theta(\infty) = 0, \end{gathered} \tag{11}$$

where $\delta = (c/\nu)^{1/2}L$ is the dimensionless velocity slip parameters $\gamma = (c/\nu)^{1/2}S$ is the dimensionless thermal slip parameter. It is to be noted that when the non-Newtonian (Casson) parameter $\beta \to \infty$, the Casson flow problem reduces to viscous flow problem.

The physical quantities of interest are the skin friction coefficient C_F and the local Nusselt number Nu_x, which are defined as

$$C_F = \frac{\tau_w}{\rho u_w^2(x)}, \qquad \mathrm{Nu}_x = \frac{xq_w}{k(T_w - T_\infty)}, \tag{12}$$

where τ_w is the shear stress along the stretching surface and q_w is the heat flux from the stretching surface, which are given by

$$\tau_w = \left(k_c + \frac{\tau_0}{\sqrt{2\pi_c}}\right)\left(\frac{\partial u}{\partial y}\right)_{y=0}, \qquad q_w = -k\left(\frac{\partial T}{\partial y}\right)_{y=0}. \tag{13}$$

Hence using (8) we get

$$\mathrm{Re}_x^{1/2}C_F = \left(1 + \frac{1}{\beta}\right)F''(0), \qquad \frac{\mathrm{Nu}_x}{\mathrm{Re}_x^{1/2}} = -\theta'(0), \tag{14}$$

where $\mathrm{Re}_x = u_w(x)x/\nu$ is the local Reynolds number.

3. Analytical Solutions for $F(\eta)$ and $\theta(\eta)$

For the explicit analytical solution of (9)–(11) by Homotopy Analysis Method (HAM), the velocity $F(\eta)$ and the temperature $\theta(\eta)$ distributions can be expressed by the set of base functions

$$\{\eta^m \exp(-n\eta) : m \geq 0,\ n \geq 0 \text{ are integers}\} \tag{15}$$

in the form:

$$\begin{gathered} F(\eta) = a_{0,0}^0 + \sum_{n=0}^{\infty}\sum_{m=0}^{\infty} a_{k,n}^m \eta^m \exp(-n\eta), \\ \theta(\eta) = \sum_{n=0}^{\infty}\sum_{m=0}^{\infty} b_{k,n}^m \eta^m \exp(-n\eta), \end{gathered} \tag{16}$$

where $a_{k,n}^m$ and $b_{k,n}^m$ are coefficients. Then from (16) and the boundary conditions (11), it is straightforward to choose

$$\begin{gathered} F_0(\eta) = \alpha\eta + \left(\frac{1-\alpha}{1+\delta}\right)[1 - \exp(-\eta)], \\ \theta_0(\eta) = \frac{\exp(-\eta)}{1+\gamma}, \end{gathered} \tag{17}$$

as our initial approximations for $F(\eta)$ and $\theta(\eta)$, respectively. We choose the auxiliary linear operators as

$$\begin{gathered} L_F(F) = \frac{\partial^3 F}{\partial \eta^3} + \frac{\partial^2 F}{\partial \eta^2}, \\ L_\theta(\theta) = \frac{\partial^2 \theta}{\partial \eta^2} - \theta, \end{gathered} \tag{18}$$

with the properties

$$L_F\left[C_1 + C_2\eta + C_3\exp(-\eta)\right] = 0,$$
$$L_\theta\left[C_4\exp(\eta) + C_5\exp(-\eta)\right] = 0, \tag{19}$$

where C_i ($i = 1-5$) are constants. Let $q \in [0,1]$ be an embedding parameter and h_F, h_θ denote the nonzero auxiliary linear operators, then the zeroth order deformation equations are

$$(1-q)L_F\left[\widehat{F}(\eta;q) - F_0(\eta)\right] = qh_F N_F\left[\widehat{F}(\eta;q)\right],$$
$$(1-q)L_\theta\left[\widehat{\theta}(\eta;q) - \theta_0(\eta)\right] = qh_\theta N_\theta\left[\widehat{F}(\eta;q), \widehat{\theta}(\eta;q)\right], \tag{20}$$

subject to the boundary conditions

$$\widehat{F}(\eta;q)\Big|_{\eta=0} = 0,$$
$$\frac{\partial\widehat{F}(\eta;q)}{\partial\eta}\Big|_{\eta=0} = 1 + \delta\frac{\partial^2\widehat{F}(\eta;q)}{\partial\eta^2}\Big|_{\eta=0}, \tag{21}$$
$$\frac{\partial\widehat{F}(\eta;q)}{\partial\eta}\Big|_{\eta=+\infty} = \frac{a}{c},$$

$$\widehat{\theta}(\eta;q)\Big|_{\eta=0} = 1 + \gamma\frac{\partial\widehat{\theta}(\eta;q)}{\partial\eta}\Big|_{\eta=0}, \qquad \widehat{\theta}(\eta;q)\Big|_{\eta=\infty} = 0, \tag{22}$$

where the nonlinear operators N_F and N_θ are defined as

$$\begin{aligned} N_F&\left[\widehat{F}(\eta;q)\right] \\ &= \left(1+\frac{1}{\beta}\right)\frac{\partial^3\widehat{F}(\eta;q)}{\partial\eta^3} + \widehat{F}(\eta;q)\frac{\partial^2\widehat{F}(\eta;q)}{\partial\eta^2} \\ &\quad - \left(\frac{\partial\widehat{F}(\eta;q)}{\partial\eta}\right)^2 + \alpha^2 + M\left[\alpha - \frac{\partial\widehat{F}(\eta;q)}{\partial\eta}\right], \\ N_\theta&\left[\widehat{F}(\eta;q), \widehat{\theta}(\eta;q)\right] \\ &= \frac{1}{\Pr}\frac{\partial^2\widehat{\theta}(\eta;q)}{\partial\eta^2} + \widehat{F}(\eta;q)\frac{\partial\widehat{\theta}(\eta;q)}{\partial\eta} - 2\frac{\partial\widehat{F}(\eta;q)}{\partial\eta}\widehat{\theta}(\eta;q) \\ &\quad + \left(1+\frac{1}{\beta}\right)E_c\frac{\partial^2\widehat{F}(\eta;q)}{\partial\eta^2} + ME_c\left(\alpha - \frac{\partial\widehat{F}(\eta;q)}{\partial\eta}\right)^2. \end{aligned} \tag{23}$$

When $q = 0$, we have from (20) that

$$\widehat{F}(\eta,0) = F_0(\eta), \qquad \widehat{\theta}(\eta,0) = \theta_0(\eta). \tag{24}$$

When $q = 1$, the zeroth order deformation equations (20)–(22) are equivalent to the original equations (9)–(11) so that we have

$$\widehat{F}(\eta,1) = F(\eta), \qquad \widehat{\theta}(\eta,1) = \theta(\eta). \tag{25}$$

So as the embedding parameter q increases from 0 to 1, $\widehat{F}(\eta,q)$ and $\widehat{\theta}(\eta,q)$ vary from their initial approximations $F_0(\eta)$ and $\theta_0(\eta)$ to their exact solutions $F(\eta)$ and $\theta(\eta)$, respectively. Expanding $\widehat{F}(\eta,q)$ and $\widehat{\theta}(\eta,q)$ in Taylor series with respect to the embedding parameter q, we can write

$$\widehat{F}(\eta,q) = F_0(\eta) + \sum_{m=1}^{\infty}F_m(\eta)q^m, \tag{26}$$

$$\widehat{\theta}(\eta,q) = \theta_0(\eta) + \sum_{m=1}^{\infty}\theta_m(\eta)q^m, \tag{27}$$

where

$$F_m(\eta) = \frac{1}{m!}\frac{\partial^m\widehat{F}(\eta;q)}{\partial q^m}\Big|_{q=0}, \qquad \theta_m(\eta) = \frac{1}{m!}\frac{\partial^m\widehat{\theta}(\eta;q)}{\partial q^m}\Big|_{q=0}. \tag{28}$$

Note that the zero order deformation equations (20) contain nonzero auxiliary parameters h_F and h_θ, respectively. Thus $\widehat{F}(\eta,q)$ and $\widehat{\theta}(\eta,q)$ are dependent upon these parameters. Assume that h_F and h_θ are so chosen that the series (26) and (27) are convergent at $q = 1$. Hence we have from (25)–(27),

$$F(\eta) = F_0(\eta) + \sum_{m=1}^{\infty}F_m(\eta),$$
$$\theta(\eta) = \theta_0(\eta) + \sum_{m=1}^{\infty}\theta_m(\eta). \tag{29}$$

Differentiating the zeroth-order deformation equations (20)–(22) m times with respect to q and then dividing by $m!$ and finally setting $q = 0$, we have the mth order deformation equations as

$$L_F\left[F_m(\eta) - \chi_m F_{m-1}(\eta)\right] = h_F R_m^F(\eta), \tag{30}$$

$$L_\theta\left[\theta_m(\eta) - \chi_m\theta_{m-1}(\eta)\right] = h_\theta R_m^\theta(\eta), \tag{31}$$

$$F_m(0) = F_m'(0) - \delta F_m''(0) = F_m'(\infty) = 0,$$
$$\theta_m(0) - \gamma\theta_m'(0) = \theta_m(\infty) = 0, \tag{32}$$

where

$$R_m^F(\eta) = \left(1+\frac{1}{\beta}\right)F''' + \sum_{k=0}^{m-1}\left[F_{m-1-k}F_k'' - F_{m-1-k}'F_k'\right] - MF_{m-1}' + \left(M\alpha+\alpha^2\right)(1-\chi_m),$$

$$R_m^\theta(\eta) = \frac{1}{\Pr}\theta_{m-1}'' + \sum_{k=0}^{m-1}F_{m-1-k}\theta_k' - 2\sum_{k=0}^{m-1}F_{m-1-k}'\theta_k + \left(1+\frac{1}{\beta}\right)E_c\sum_{k=0}^{m-1}F_{m-1-k}''F_k'' + (1-\chi_m)ME_c\alpha^2 - 2ME_c\alpha F_{m-1}' + ME_c\sum_{k=0}^{m-1}F_{m-1-k}'F_k', \quad (33)$$

$$\chi_m = \begin{cases} 0 & m \le 1 \\ 1 & m \ge 2. \end{cases}$$

The general solutions of (30)–(32) are

$$F_m(\eta) = F_m^*(\eta) + C_1 + C_2\eta + C_3\exp(-\eta),$$
$$\theta_m(\eta) = \theta_m^*(\eta) + C_4\exp(\eta) + C_5\exp(-\eta), \quad (34)$$

where $F_m^*(\eta)$ and $\theta_m^*(\eta)$ denote the special solutions of (30) and (31) and the integral constants C_i $(i = 1,2,3,4,5)$ are determined by the following boundary conditions:

$$C_2 = C_4 = 0, \quad C_3 = \frac{1}{1+\delta}\left[\left.\frac{\partial F_m^*(\eta)}{\partial\eta}\right|_{\eta=0} - \delta\left.\frac{\partial^2 F_m^*(\eta)}{\partial\eta^2}\right|_{\eta=0}\right],$$
$$C_1 = -C_3 - F_m^*(0), \quad C_5 = \frac{1}{1+\gamma}\left[\gamma\left.\frac{\partial\theta_m^*(\eta)}{\partial\eta}\right|_{\eta=0} - \theta_m^*(0)\right]. \quad (35)$$

The linear mth order deformation equations (30) and (31) can be solved one after the other by using the symbolic computation software MATHEMATICA.

4. Convergence of the HAM Solution

Equation (29) gives the analytical solution of the problem in series form. As pointed out by Liao [35], the convergence region and rate of convergence of the solution series given by HAM depend upon auxiliary parameters h_F and h_θ. Hence these auxiliary parameters provide us with a convenient way to adjust and control the convergence region and rate of the solution series. To select appropriate values of these parameters, we display the so called h_F and h_θ curves at 20th order approximations. Figure 2 reveals that there exists horizontal line segment for $(h_F, F''(0))$ curves in $-0.8 \le h_F \le -0.3$ and for $(h_\theta, \theta''(0))$ curve in $-0.85 \le h_\theta \le 0.25$. The obtained series solutions given by (29) converge in the whole region of η when $h_F = h_\theta = -0.3$. Here we have employed the homotopy-Pade approximation (see Mahapatra et al. [40]) instead of traditional-Pade approximation for the rapid convergence of the series solutions. Table 1 is made to show the convergence of the solutions for $F''(0)$ and $-\theta'(0)$ using homotopy-Pade approximation.

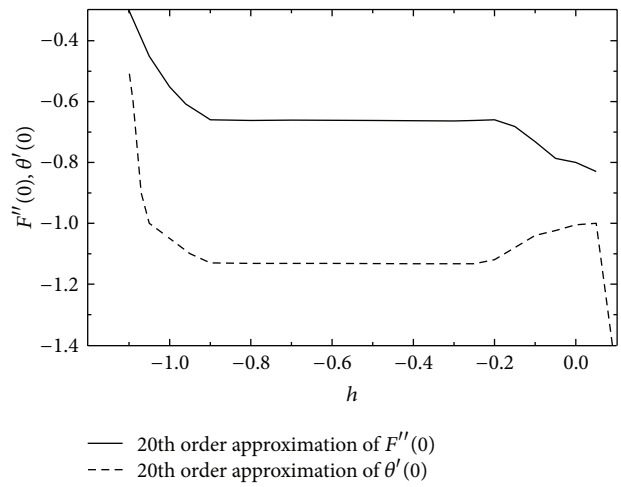

Figure 2: h curve for $F''(0)$ and $\theta'(0)$.

Table 1: Convergence solution for different order of approximations when $\beta = 1.0$, $\alpha = 0.5$, $M = 1.0$, $\delta = 0.5$, $\Pr = 0.7$, $\gamma = 0.3$, and $E_c = 0.1$.

Order of approximations	$-F''(0)$	$-\theta'(0)$
1	0.302781	0.405632
5	0.342341	0.437431
10	0.362178	0.457285
20	0.362489	0.457285
30	0.362489	0.457285
40	0.362489	0.457285

5. Results and Discussion

Equations (9) and (10) subject to the boundary conditions (11) are solved analytically for some values of the governing parameters β, α, M, Pr, E_c, δ, and γ. In order to verify the accuracy of the present method, we have compared our results with those of Mahapatra and Gupta [4] and Ishak et al. [6] for the skin friction coefficient $F''(0)$ for different values of α (in the case of $\beta \to \infty$, $M = 0$ and $\delta = 0$) in Table 2. The comparison shows good agreement for each value of α. Therefore, the present results obtained are accurate enough.

This section describes the influence of some important physical parameters on the velocity and thermal profiles. For this purpose, Figures 3–11 are displayed. Attention is focussed on variations of the velocity slip parameter δ, the magnetic parameter M, the thermal slip parameter γ, the casson parameter β, the velocity ratio parameter α, and the Prandtl number Pr on the velocity and the temperature distributions.

Figure 3 shows the influence of δ on the velocity component F'. It is observed that F' is a decreasing function of the slip parameter δ. Physically this is explained as follows: when

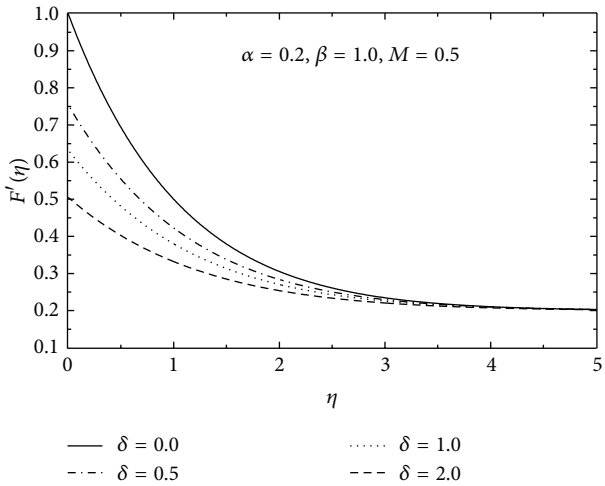

Figure 3: Influence of the velocity slip parameter δ on F'.

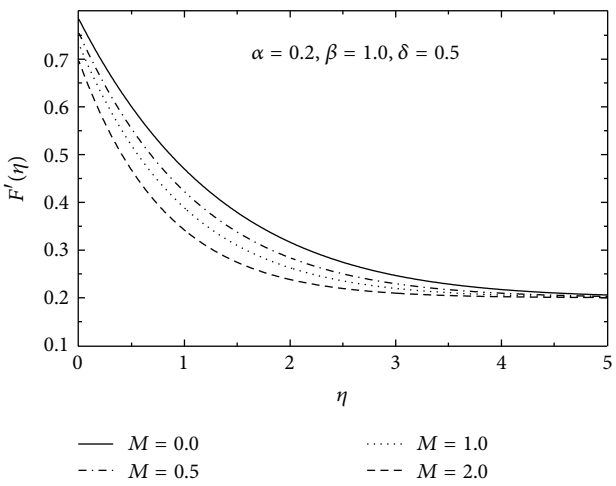

Figure 4: Influence of the magnetic parameter M on F'.

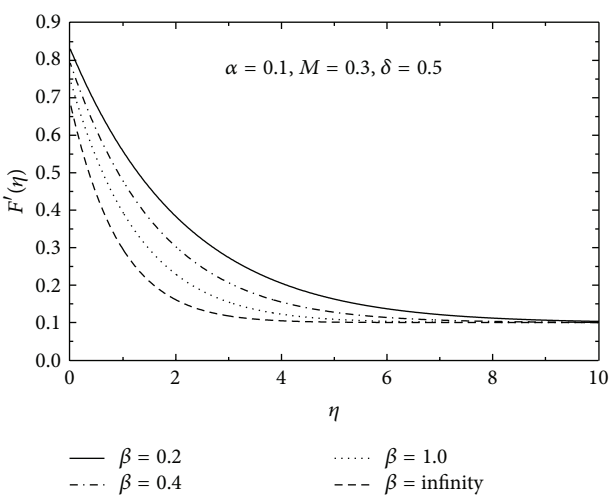

Figure 5: Influence of the Casson parameter β on F'.

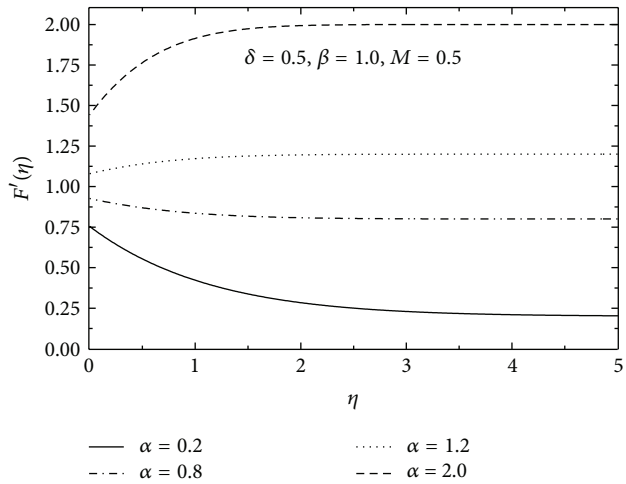

Figure 6: Influence of the velocity ratio parameter α on F'.

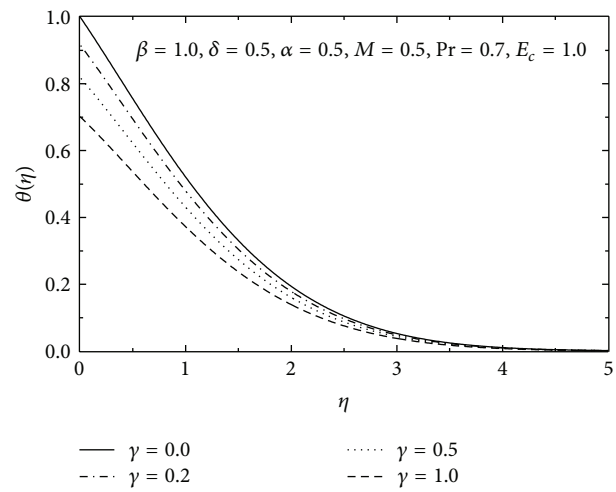

Figure 7: Influence of the thermal slip parameter γ on $\theta(\eta)$.

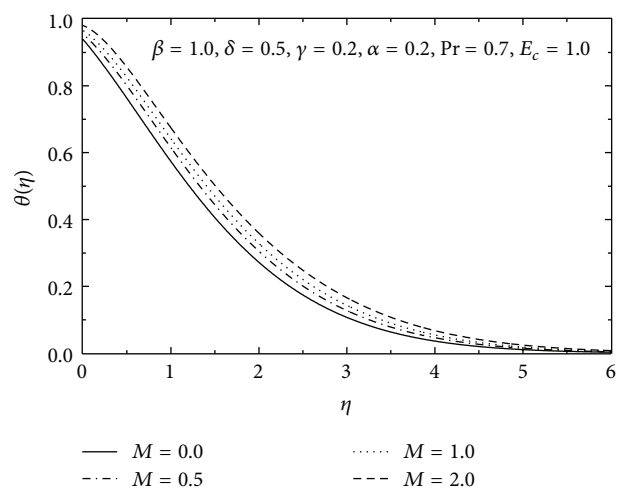

Figure 8: Influence of the magnetic parameter M on $\theta(\eta)$.

Table 2: Comparison of the values of $F''(0)$ (with $\beta \to \infty$) for different values of $\alpha(=a/c)$ with $M = 0$ and $\delta = 0$.

α	Present study	Mahapatra and Gupta [4]	Ishak et al. [6]
0.01	−0.998024	—	−0.9980
0.10	−0.969386	−0.9694	−0.9694
0.20	−0.918107	−0.9181	−0.9181
0.50	−0.667264	−0.6673	−0.6673
1.0	0	0	0
2.0	2.017507	2.0175	2.0175

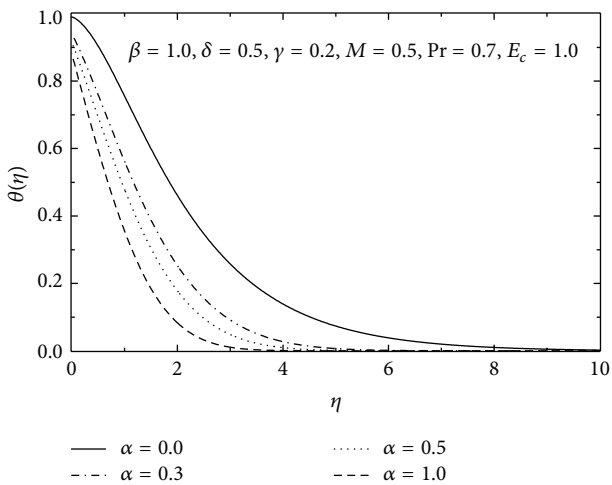

Figure 9: Influence of the velocity ratio parameter α on $\theta(\eta)$.

slip occurs (for nonzero value of δ), the fluid velocity near the sheet is no longer equal to the sheet stretching velocity; that is, a velocity slip exists. With the increase in δ, such a slip velocity increases. Furthermore, increasing the value of δ will decrease the flow velocity because under the slip condition, the pulling of the stretching sheet can be only partly transmitted to the fluid. The boundary layer thickness also decreases as the slip parameter δ increases. The effect of the magnetic field parameter M on velocity F' is depicted in Figure 4. From this figure, it is observed that the transverse magnetic field contributes to the reduction in the velocity profile and boundary later thickness. This is evident from the fact that applied transverse magnetic field produces a body force, to be precise, the Lorentz force, which opposes the motion. The resistance offered to the flow is responsible in decreasing the fluid velocity. The influence of the Casson parameter β on the velocity profile is displayed in Figure 5. The figure reveals that as β increases, the velocity and the boundary layer thickness decrease. Hence, it is quite obvious that the magnitude of the velocity is greater in casson fluid when compared with the viscous fluid. The effect of the velocity ratio parameter α on the velocity field F' is shown in Figure 6. The figure indicates that fluid velocity increases with the increase of α.

To see the variations of γ, M, α, Pr (Prandtl number), and E_c(Eckert number) on the temperature profile θ, Figures 7–11 are plotted. The effect of the thermal slip parameter γ

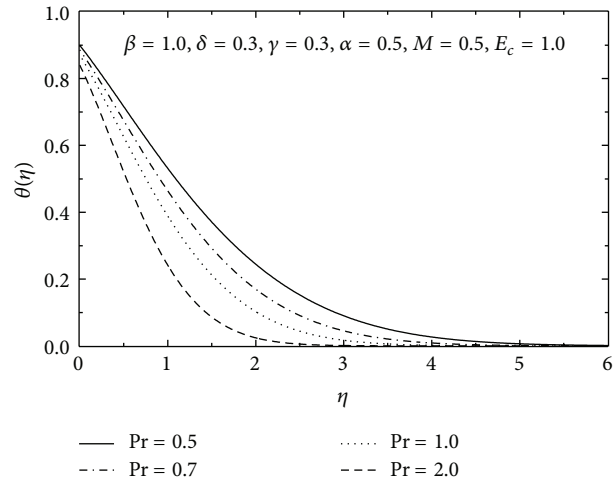

Figure 10: Influence of the Prandtl number Pr on $\theta(\eta)$.

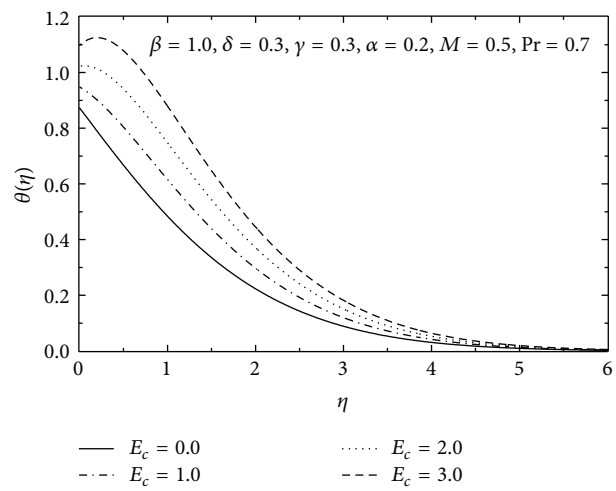

Figure 11: Influence of the Eckert number E_c on $\theta(\eta)$.

on temperature distribution is displayed in Figure 7. As the thermal slip increases, less heat is transferred from the sheet to the fluid and consequently the temperature decreases. Figure 8 depicts the effect of M on temperature θ. It is observed that temperature and the thermal boundary layer thickness increase with increasing M. Figure 9 exhibits the temperature profile θ for different values of the velocity ratio parameter α. The figure shows that the temperature and the thermal boundary layer thickness decrease with an increase in α. Hence, stronger free stream velocity causes a reduction in the temperature and the thermal boundary layer thickness.

Figure 10 demonstrates the effect of the Prandtl number Pr on the temperature profile θ. The temperature and the thermal boundary layer thickness decrease with the increase of Pr. Physically this is explained as follows. An increase in the Prandtl number means an increase of fluid viscosity, which causes a decrease in the temperature distribution. An enhancement in the Eckert number E_c results in an increase in temperature θ, and this observation can easily be visualized in Figure 11.

Table 3: Values of $F''(0)$ for different values of β, M, and α with $\delta = 0.5$.

β	M	$\alpha \rightarrow$ 0.01	0.2	0.5	1.5	2.0
0.5	0.1	−0.426217	−0.386951	−0.275757	0.353516	0.762695
	0.5	−0.486374	−0.427637	−0.296141	0.365707	0.782862
	1.0	−0.546294	−0.469744	−0.317999	0.379546	0.806099
1.0	0.1	−0.491127	−0.445542	−0.316722	0.401925	0.863115
	0.5	−0.558715	−0.490648	−0.338915	0.414637	0.883828
	1.0	−0.625100	−0.536776	−0.362489	0.428997	0.907599

Table 4: Values of $-\theta'(0)$ for different values of β, M, and Pr with $\delta = 0.5$, $\gamma = 0.3$, $\alpha = 0.2$, and $E_c = 0.1$.

β	M	Pr $\rightarrow$ 0.1	0.5	0.71	2.0	5.0
0.5	0.1	0.147355	0.355671	0.423755	0.675504	0.956279
	0.5	0.141579	0.340118	0.404804	0.646344	0.912599
	1.0	0.136239	0.324898	0.386483	0.616944	0.868322
1.0	0.1	0.140813	0.341966	0.409257	0.662231	0.948732
	0.5	0.135781	0.327236	0.391145	0.634582	0.908910
	1.0	0.131151	0.312713	0.374024	0.607155	0.869149

Tables 3 and 4 show the variation of the reduced skin friction coefficient $F''(0)$ and the coefficient of the reduced Nusselt number $-\theta'(0)$ for different values of the physical parameters β, M, α, and Pr considering other parameters fixed. From Table 3, it is observed that $|F''(0)|$ is an increasing function of the dimensionless parameters β and M. Also $|F''(0)|$ decreases with the increase of α as long as $\alpha < 1$ and increases with the increase of α for $\alpha > 1$. Table 4 reveals that $-\theta'(0)$ is a decreasing function of β and M while an increasing function of Pr.

6. Conclusion

The present work considers the hydromagnetic steady flow and heat transfer of a non-Newtonian casson fluid in the neighborhood of a stagnation point over a stretching surface with partial slip at the boundary. The governing equations are formulated and transformed into a set of ordinary differential equations by similarity transformation. The resulting equations are solved analytically using homotopy analysis method. The main points of this study are as follows.

(i) The velocity F' decreases with increasing values of δ, M, and β.

(ii) The temperature θ decreases with increasing values of γ, α, and Pr, and increases with increasing values of M and E_c.

(iii) The magnitude of velocity is greater in case of Casson fluid when compared with the viscous fluid.

(iv) Increase of the velocity slip parameter δ causes decrease in the flow velocity, and the same qualitative result holds for the thermal slip parameter γ on the temperature.

(v) The present results in limiting cases ($\beta \rightarrow \infty$, $M = 0$, $\delta = 0$) are found in excellent agreement with those of Mahapatra and Gupta [4] and Ishak et al. [6].

Acknowledgment

The author thanks the referees for their valuable comments and suggestions which enabled and improved presentation of the paper.

References

[1] B. C. Sakiadis, "Boundary layer equations for the two-dimensional and axi-symmetric flow," *AIChE Journal*, vol. 7, pp. 26–28, 1961.

[2] T. C. Chiam, "Stagnation-point flow towards a stretching plate," *Journal of the Physical Society of Japan*, vol. 63, no. 6, pp. 2443–2444, 1994.

[3] T. R. Mahapatra and A. S. Gupta, "Magnetohydrodynamic stagnation-point flow towards a stretching sheet," *Acta Mechanica*, vol. 152, no. 1–4, pp. 191–196, 2001.

[4] T. R. Mahapatra and A. S. Gupta, "Heat transfer in stagnation-point flow towards a stretching sheet," *Heat and Mass Transfer*, vol. 38, no. 6, pp. 517–521, 2002.

[5] M. Reza and A. S. Gupta, "Steady two-dimensional oblique stagnation-point flow towards a stretching surface," *Fluid Dynamics Research*, vol. 37, no. 5, pp. 334–340, 2005.

[6] A. Ishak, R. Nazar, N. M. Arifin, and I. Pop, "Mixed convection of the stagnation-point flow towards a stretching vertical permeable sheet," *Malaysian Journal of Mathematical Sciences*, vol. 2, pp. 217–226, 2007.

[7] C. Y. Wang, "Stagnation flow towards a shrinking sheet," *International Journal of Non-Linear Mechanics*, vol. 43, no. 5, pp. 377–382, 2008.

[8] R. A. Van Gorder, K. Vajravelu, and I. Pop, "Hydromagnetic stagnation point flow of a viscous fluid over a stretching or shrinking sheet," *Meccanica*, vol. 47, no. 1, pp. 31–50, 2012.

[9] K. R. Rajagopal, T. Y. Na, and A. S. Gupta, "Flow of a viscoelastic fluid over a stretching sheet," *Rheologica Acta*, vol. 23, no. 2, pp. 213–215, 1984.

[10] B. Siddappa and S. Abel, "Non-Newtonian flow past a stretching plate," *Zeitschrift für Angewandte Mathematik und Physik*, vol. 36, pp. 47–54, 1985.

[11] W. C. Troy, E. A. Overmannll, G. B. Eremont-Rout, and J. P. Keener, "Uniqueness of the flow of second order fluid flow past a stretching sheet," *Quarterly of Applied Mathematics*, vol. 44, pp. 753–755, 1987.

[12] P. S. Lawrence and B. N. Rao, "The nonuniqueness of the MHD flow of a viscoelastic fluid past a stretching sheet," *Acta Mechanica*, vol. 112, no. 1–4, pp. 223–225, 1995.

[13] J. B. McLeod and K. R. Rajagopal, "On the uniqueness of flow of a Navier-Stokes fluid due to a stretching boundary," *Archive for Rational Mechanics and Analysis*, vol. 98, no. 4, pp. 385–393, 1987.

[14] H. I. Andersson, "MHD flow of a viscoelastic fluid past a stretching surface," *Acta Mechanica*, vol. 95, no. 1–4, pp. 227–230, 1992.

[15] D. Rollins and K. Vajravelu, "Heat transfer in a second-order fluid over a continuous stretching surface," *Acta Mechanica*, vol. 89, no. 1–4, pp. 167–178, 1991.

[16] M. S. Abel and P. Veena, "Viscoelastic fluid flow and heat transfer in a porous medium over a stretching sheet," *International Journal of Non-Linear Mechanics*, vol. 33, no. 3, pp. 531–538, 1998.

[17] W. P. Walawender, T. Y. Chen, and D. F. Cala, "An approximate casson fluid model for tube flow of blood," *Biorheology*, vol. 12, no. 2, pp. 111–124, 1975.

[18] G. W. S. Blair, "An equation for the flow of blood, plasma and serum through glass capillaries," *Nature*, vol. 183, no. 4661, pp. 613–614, 1959.

[19] S. Charm and G. Kurland, "Viscometry of human blood for shear rates of 0–100,000 sec^{-1}

," *Nature*, vol. 206, no. 4984, pp. 617–618, 1965.

[20] E. W. Merrill, A. M. Benis, E. R. Gilliland, T. K. Sherwood, and E. W. Salzman, "Pressure-flow relations of human blood in hollow fibers at low flow rates," *Journal of Applied Physiology*, vol. 20, no. 5, pp. 954–967, 1965.

[21] D. A. Mc Donald, *Blood Flows in Arteries*, chapter 2, Arnold, London, UK, 2nd edition, 1974.

[22] C. Y. Wang, "Flow due to a stretching boundary with partial slip—an exact solution of the Navier-Stokes equations," *Chemical Engineering Science*, vol. 57, no. 17, pp. 3745–3747, 2002.

[23] H. I. Andersson, "Slip flow past a stretching surface," *Acta Mechanica*, vol. 158, no. 1-2, pp. 121–125, 2002.

[24] S. Mukhopadhyay and H. I. Andersson, "Effects of slip and heat transfer analysis of flow over an unsteady stretching surface," *Heat and Mass Transfer*, vol. 45, no. 11, pp. 1447–1452, 2009.

[25] T. Fang, J. Zhang, and S. Yao, "Slip MHD viscous flow over a stretching sheet—an exact solution," *Communications in Nonlinear Science and Numerical Simulation*, vol. 14, no. 11, pp. 3731–3737, 2009.

[26] S. Mukhopadhyay, "Effects of slip on unsteady mixed convective flow and heat transfer past a stretching surface," *Chinese Physics Letters*, vol. 27, no. 12, Article ID 124401, 2010.

[27] T. Fang, S. Yao, J. Zhang, and A. Aziz, "Viscous flow over a shrinking sheet with a second order slip flow model," *Communications in Nonlinear Science and Numerical Simulation*, vol. 15, no. 7, pp. 1831–1842, 2010.

[28] T. Fang, J. Zhang, and S. Yao, "Slip magnetohydrodynamic viscous flow over a permeable shrinking sheet," *Chinese Physics Letters*, vol. 27, no. 12, Article ID 124702, 2010.

[29] K. Bhattacharyya, S. Mukhopadhyay, and G. C. Layek, "Slip effects on boundary layer stagnation-point flow and heat transfer towards a shrinking sheet," *International Journal of Heat and Mass Transfer*, vol. 54, no. 1–3, pp. 308–313, 2011.

[30] K. Bhattacharyya, S. Mukhopadhyay, and G. C. Layek, "MHD boundary layer slip flow and heat transfer over a flat plate," *Chinese Physics Letters*, vol. 28, no. 2, Article ID 024701, 2011.

[31] P. D. Ariel, T. Hayat, and S. Asghar, "The flow of an elastico-viscous fluid past a stretching sheet with partial slip," *Acta Mechanica*, vol. 187, no. 1–4, pp. 29–35, 2006.

[32] P. D. Ariel, "Two dimensional stagnation point flow of an elastico-viscous fluid with partial slip," *Zeitschrift für Angewandte Mathematik und Physik*, vol. 88, no. 4, pp. 320–324, 2008.

[33] T. Fang, J. Zhang, and S. Yao, "Slip MHD viscous flow over a stretching sheet—an exact solution," *Communications in Nonlinear Science and Numerical Simulation*, vol. 14, no. 11, pp. 3731–3737, 2009.

[34] S. J. Liao, *On the proposed homotopy analysis techniques for nonlinear problems and its applications [Ph.D. thesis]*, Shanghai Jiao Tong University, Shanghai, China, 1992.

[35] S. J. Liao, *Homotopy Analysis Method in Nonlinear Differential Equations*, Higher Education Press, Beijing, China; Springer, Berlin, Germany, 2012.

[36] S. Liao, "An analytic solution of unsteady boundary-layer flows caused by an impulsively stretching plate," *Communications in Nonlinear Science and Numerical Simulation*, vol. 11, no. 3, pp. 326–339, 2006.

[37] T. Hayat, Z. Abbas, and M. Sajid, "Series solution for the upper-convected Maxwell fluid over a porous stretching plate," *Physics Letters A*, vol. 358, no. 5-6, pp. 396–403, 2006.

[38] S. Liao, "Notes on the homotopy analysis method: some definitions and theorems," *Communications in Nonlinear Science and Numerical Simulation*, vol. 14, no. 4, pp. 983–997, 2009.

[39] R. A. Van Gorder and K. Vajravelu, "On the selection of auxiliary functions, operators, and convergence control parameters in the application of the Homotopy Analysis Method to nonlinear differential equations: a general approach," *Communications in Nonlinear Science and Numerical Simulation*, vol. 14, no. 12, pp. 4078–4089, 2009.

[40] T. R. Mahapatra, S. K. Nandy, and A. S. Gupta, "Analytical solution of magnetohydrodynamic stagnation-point flow of a power-law fluid towards a stretching surface," *Applied Mathematics and Computation*, vol. 215, no. 5, pp. 1696–1710, 2009.

[41] S. Abbasbandy, "Homotopy analysis method for the Kawahara equation," *Nonlinear Analysis: Real World Applications*, vol. 11, no. 1, pp. 307–312, 2010.

[42] M. Nakamura and T. Sawada, "Numerical study on the flow of a non-Newtonian fluid through an axisymmetric stenosis," *Journal of Biomechanical Engineering*, vol. 110, no. 2, pp. 137–143, 1988.

[43] J. A. Shercliff, *A Textbook of Magnetohydrodynamics*, Pergamon Press, Oxford, UK, 1965.